JOURNAL OF APPLIED ELECTROCHEMISTRY 14 (1984) 165–175

The mechanism of oxidation of copper in alkaline solutions

M. R. GENNERO DE CHIALVO, S. L. MARCHIANO, A. J. ARVÍA

Instituto de Investigaciones Fisicoquímicas Teóricas y Aplicadas – INIFTA – Casilla de Correo 16, Sucursal 4, 1900 La Plata, Argentina

Received 11 March 1983

The formation of Cu_2O by the oxidation of Cu in alkaline solutions under various controlled potential conditions has been studied by potentiodynamic methods, the rotating ring disc technique and by employing colloidal $Cu(OH)_2$ electrodes supported on vitreous carbon.

The kinetics of the electrochemical reactions, both anodic and cathodic, are interpreted in terms of a complex reaction mechanism involving various intermediates participating in the phase oxide formation, (e.g. adsorbed OH, soluble Cu(I) and metal sites of different activity).

Besides the electrochemical reactions the model includes various ageing and surface restructuring processes. The growth mechanism is envisaged to depend on the conditions of oxidation.

1. Introduction

The literature on the electro-oxidation of Cu to Cu_2O in alkaline electrolytes covering both the kinetics and the structural aspects of the reaction shows some disagreements, in part, because the overall electrochemical process is more involved than thought earlier [1–10]. The same situation is apparent for the electro-reduction of Cu_2O to Cu, particularly when this reaction proceeds during a potential sweep. The variation in the results is due to differences in the Cu electrode history, principally the electrode pretreatment and the parameters defining the potential perturbation conditions [10–12]. Thus, the apparent discrepancies in the published data concerning the relative importance and number of potentiodynamic current peaks associated with the cathodic reactions and the mechanisms proposed to interpret their kinetics should be attributed to a lack of complete control of the experimental conditions.

Previous data have qualitatively shown that the layer electroformed on polycrystalline Cu undergoes some structural rearrangements related to ageing effects [7, 10, 12]. On the other hand, the multiplicity of the electro-reduction profile and the relative contribution of the different current peaks depends also on the thickness and history of the Cu_2O layer. From these results the participation of the disproportionation reactions of Cu(I) yielding Cu(II) and Cu(0) species, the simultaneous formation of Cu(II) species in the potential range of the Cu to Cu_2O oxidation and the occurrence of both aged and non-aged O-containing species were envisaged [10].

The present work confirms the presence of soluble Cu ionic species during the electro-oxidation of Cu to Cu_2O and establishes the optimal conditions in which these species can be detected. In addition, the influence of these species on the *E/I* curves is reported. From the present results and from previous data a more detailed mechanism for the complex electrochemical reactions of Cu in alkaline solution in the potential range for Cu_2O electroformation and electro-reduction is presented.

2. Experimental details

Experiments were run with a conventional three compartment, Pyrex glass cell. The working electrode was either a polycrystalline Cu wire (99.9% purity, 0.322 cm^2 apparent area) held in a PTFE rod or a Cu disc (99.9% purity, 0.0314 cm^2 apparent area) axially mounted in a PTFE rod. The counterelectrode consisted of a large area Pt

0021-891X/84 $03.00 + .12

plate (4.0 cm^2). A Hg/HgO/1 mol dm^{-3} NaOH reference electrode connected through a Luggin capillary tip was employed ($E^0 = 100$ mV vs NHE). In the text, the potentials are referred to the NHE scale after correcting for the liquid junction potential. The working electrode pretreatment consisted of gradual mechanical polishing with alumina powder down to 0.3 μm particle size, and multiple rising with triply distilled water. Occasionally, after the mechanical polishing the electrode was etched in 1:1 nitric acid–water solution for 15 s. The alkaline electrolyte, 0.01 mol $dm^{-3} < C_{NaOH} < 2$ mol dm^{-3}, was prepared from AnalaR NaOH and triply distilled water. Runs were made under purified nitrogen at 25°C.

Before each run, the working electrode was subjected to a repetitive triangular potential sweep (RTPS) between E_c(-1.1 V $< E_c < -1.0$ V), just in the range where H_2 occurs and E_a (-0.1 V $< E_a < 0.0$ V), which corresponds to the upper potential range for Cu_2O formation. Both E_c and E_a were chosen according to the NaOH electrolyte concentration. Under these conditions the RTPS was continued until a steady state profile was attained. Afterwards, the appropriate combination of linear potential sweep and potential step were applied to the working electrode. The various perturbation programmes are depicted on the figures with the resulting E/I profiles. The potential step (E_s) covering the Cu(I) electroformation potential range, lasted between $0 < \tau < 180$ s. The potential sweep rate (v_s) was varied between 0.01 and 0.5 V s^{-1}.

To identify the soluble Cu ionic species formed during the electro-oxidation of Cu to Cu(I) an Au-ring (0.035 cm^2 apparent area) Cu-disc (0.125 cm^2 apparent area) rotating electrode was used (collection efficiency 0.25), at rotation speeds (ω) in the range $500 < \omega < 7000$ rpm. The Au-ring electrode was held at a potential in the range $-0.6 < E_r < 0.05$ V, covering the regions both positive and negative to the Cu/Cu_2O equilibrium potential. Within the chosen potential range neither water nor OH^- ion discharge occur on Au. The Cu-disc electrode was subjected to a single triangular potential sweep (TPS).

Experiments were also made by using a working electrode initially consisting of a vitreous carbon base covered with a $Cu(OH)_2$ film chemically precipitated, on the conducting substrate by alternative immersions in 1 mol dm^{-3} $CuSO_4$ and 1 mol dm^{-3} NaOH respectively. When this type of electrode is subjected to an appropriate TPS, $Cu(OH)_2$ is firstly reduced to a thin layer of Cu on vitreous carbon and later this layer is oxidized to Cu_2O. In this way it is possible, in principle, to limit the extent of the Cu to Cu_2O reaction.

3. Results

3.1. *E/I profiles run with different perturbation programmes*

The stabilized RTPS E/I profile in 0.1 mol dm^{-3} NaOH at 0.2 V s^{-1} in the range -1.025 and -0.050 V (the potential range where Cu and Cu(I) are the main Cu species participating in the electrode reactions) exhibits an anodic current peak API at *ca.* -0.135 V (E_p^{API}) and a cathodic current peak CPI at *ca.* -0.445 V (E_p^{CPI}) (Fig. 1, curve 1). The anodic charge (Q_a) is greater than the cathodic charge (Q_c) and this charge difference can be taken as a first indication that ionic Cu species in solution are also produced in the overall reaction.

When the perturbation programme includes a potential hold at E_s for time τ (Fig. 1, curve 2) the electro-reduction profile of the species anodically formed is considerably changed; it

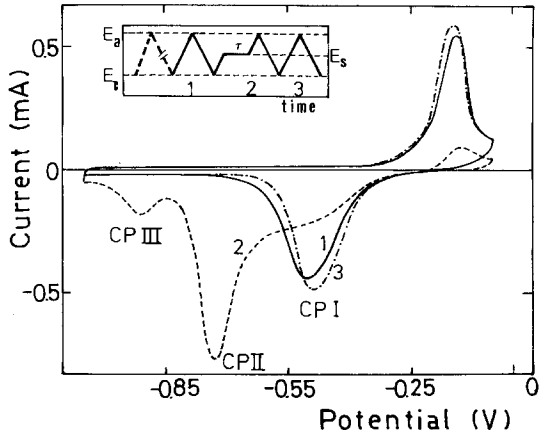

Fig. 1. Potentiodynamic E/I profiles for the potential perturbation programme depicted in the Fig. 0.1 mol dm^{-3} NaOH; $v_s = 0.2$ V s^{-1}; $E_s = -0.20$ V; $\tau = 30$ s. 1. Stabilized E/I profile; 2. first cycle after the potential step (E_s); 3. second cycle after the potential step (E_s).

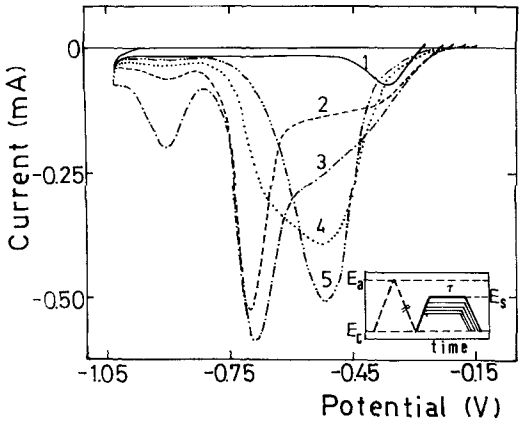

Fig. 2. Potentiodynamic E/I profile for the potential perturbation programmes involving different E_s values. 0.1 mol dm^{-3} NaOH; $v_s = 0.2$ V s^{-1}; $\tau = 30$ s. 1. $E_s = -0.275$ V; 2. $E_s = -0.225$ V; 3. $E_s = -0.200$ V; 4. $E_s = -0.175$ V; 5. $E_s = -0.150$ V.

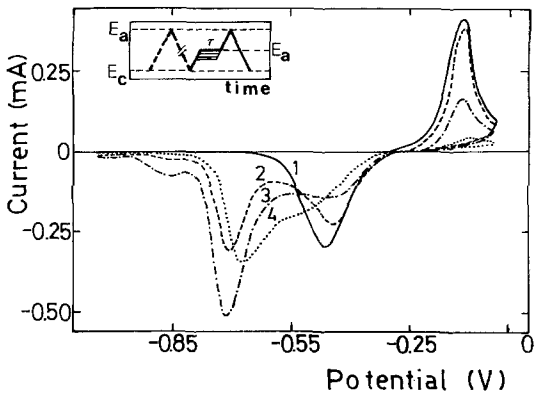

Fig. 3. Potentiodynamic E/I profile for the potential perturbation progammes shown. 0.05 mol dm^{-3} NaOH; $v_s = 0.2$ V s^{-1}; $\tau = 30$ s. 1. $E_s = -0.275$ V; 2. $E_s = -0.225$ V; 3. $E_s = -0.200$ V; 4. $E_s = -0.175$ V.

exhibits a multiplicity of peaks, whose magnitude and relative distribution depends strongly on E_c, E_s, E_a, τ, v_s and C_{NaOH}. Thus, the first negative going scan after the potential hold shows two additional peaks (CPII and CPIII) both at potentials more negative than that of CPI (Fig. 1, curve 2). However, CPII and CPIII disappear during repeated cycling and the overall profile progressively recovers its initial shape (Fig. 1, curve 3). The number of RTPS (or time) required to approach the stabilized E/I profile increases with τ.

At a constant τ, the value of E_s ($E_s < E_p^{API}$) influences considerably the characteristics of the electro-reduction profile (Fig. 2).

Thus, under the perturbation conditions shown in Fig. 2 when $-0.28 < E_s = E_a < -0.25$ V, only one broad and asymmetric cathodic peak at -0.360 V is recorded. Practically the same type of response is found when immediately after the potential hold, the anodic reaction is continued potentiodynamically before the potential scan is reversed (Fig. 3). This peak, however, is not always observed under the perturbation programme depicted in Fig. 3. When $E_s = -0.275$ V and $E_a = -0.05$ V only a single symmetric cathodic peak is seen, its peak potential being slightly more negative than E_p^{CPI}. Nevertheless, in both cases (Figs. 2 and 3), as E_s becomes more positive ($E_s > -0.225$ V) the negative going E/I profile shows peaks CPII and CPIII; the maximum splitting is observed when E_s is set at the middle of the ascending branch of API (*ca.* -0.2 V).

When $E_s = -0.2$ V $= E_a$ and $v_s = 0.2$ V s^{-1}, the electro-reduction peak multiplicity depends on τ (Fig. 4). Thus, the height of the small peak at *ca.* -0.325 V for $\tau = 0$ s, increases with τ and its potential shifts towards more negative values.

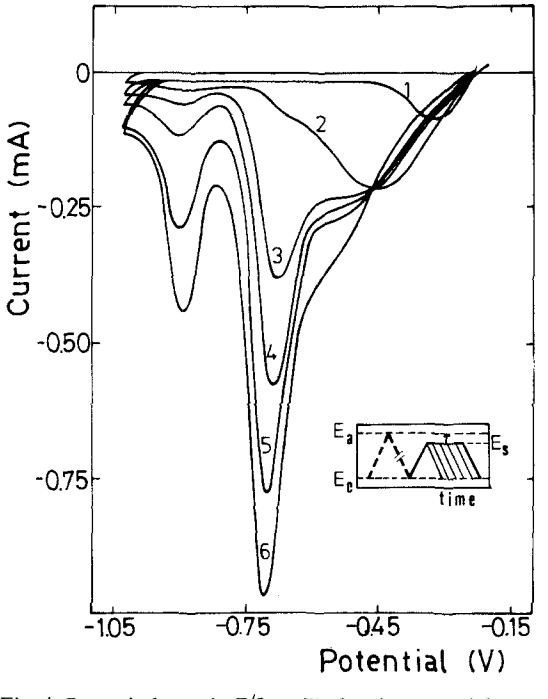

Fig. 4. Potentiodynamic E/I profile for the potential perturbation programmes with different τ. 0.1 mol dm^{-3} NaOH; $v_s = 0.2$ V s^{-1}; $E_s = -0.200$ V. 1. $\tau = 0$ s; 2. $\tau = 7$ s; 3. $\tau = 15$ s; 4. $\tau = 30$ s; 5. $\tau = 60$ s; 6. $\tau = 180$ s.

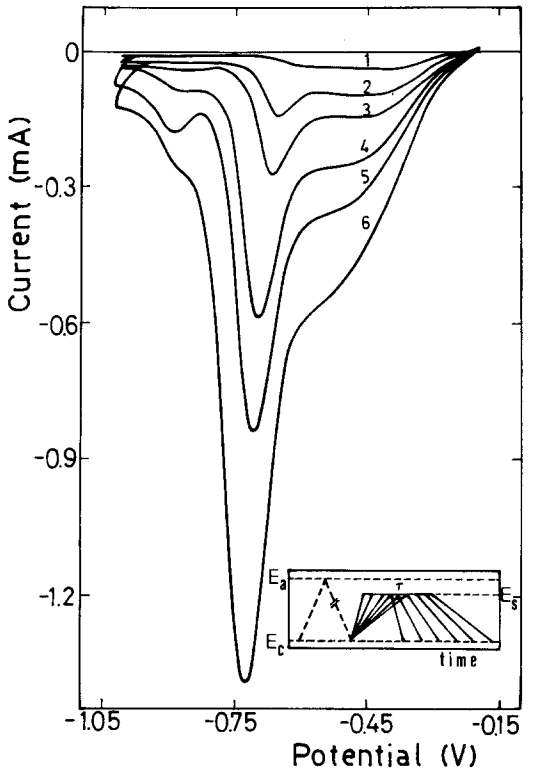

Fig. 5. Potentiodynamic E/I profile for the perturbation programmes at different v_s. 0.1 mol dm^{-3} NaOH; $\tau = 30$ s; $E_s = -0.200$ V. 1. $v_s = 0.01$ V s^{-1}; 2. $v_s = 0.05$ V s^{-1}; 3. $v_s = 0.1$ V s^{-1}; 4. $v_s = 0.2$ V s^{-1}; 5. $v_s = 0.3$ V s^{-1}; 6. $v_s = 0.5$ V s^{-1}.

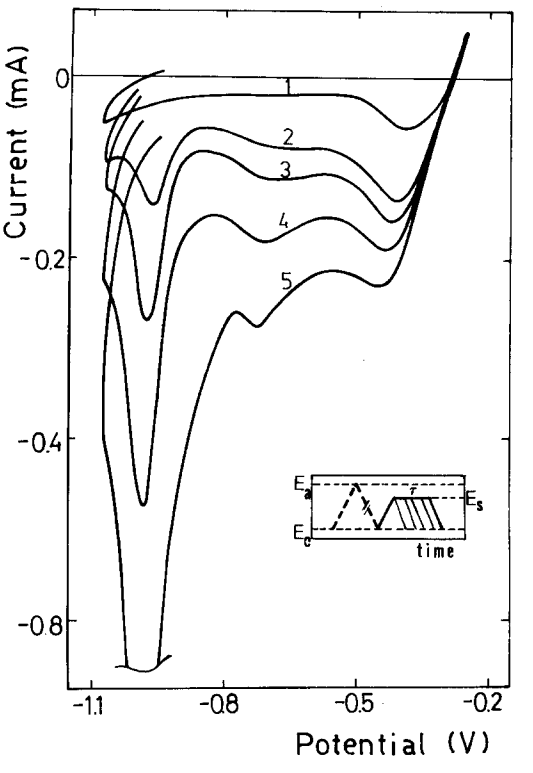

Fig. 6. Potentiodynamic E/I profile for the potential perturbation programmes with different τ values. 1 mol dm^{-3} NaOH; $v_s = 0.1$ V s^{-1}; $E_s = -0.250$ V. 1. $\tau = 0$ s; 2. $\tau = 2$ s; 3. $\tau = 5$ s; 4. $\tau = 10$ s; 5. $\tau = 20$ s.

Simultaneously as τ increases, the overall cathodic charge also increases and CPII and CPIII become the most important contributions in the voltammogram. A clear isopotential point is defined at -0.46 V which is probably related to a chemical transformation of the oxide layer. The electroreduction profile run under constant $E_s = E_a$ and τ depends on v_s (Fig. 5). For the smallest value of v_s a nearly cathodic current plateau, probably related to CPI, is observed in the range -0.3 to -0.6 V. But as v_s increases, the contributions of CPI, CPII and CPIII increase, and both E_p^{CPII} and E_p^{CPIII} gradually shift towards more negative values. Finally, for the highest v_s, CPIII is hardly observed and it appears only as a shoulder of CPII.

The relative contributions of the various cathodic peaks also depends on the electrolyte concentration (Figs. 4, 6 and 7). With both v_s and τ constant, the value of E_s corresponding to the maximum peak multiplicity (E_s^{max}) changes

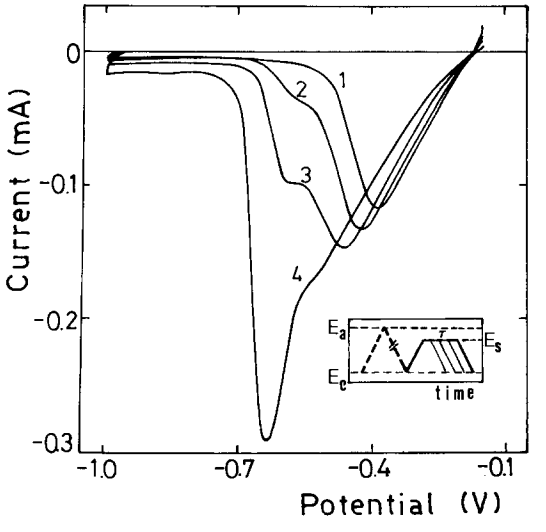

Fig. 7. Potentiodynamic E/I profile for the potential perturbation programmes with different τ values. 0.01 mol dm^{-3} NaOH; $v_s = 0.1$ V s^{-1}; $E_s = -0.150$ V. 1. $\tau = 5$ s; 2. $\tau = 10$ s; 3. $\tau = 20$ s; 4. $\tau = 60$ s.

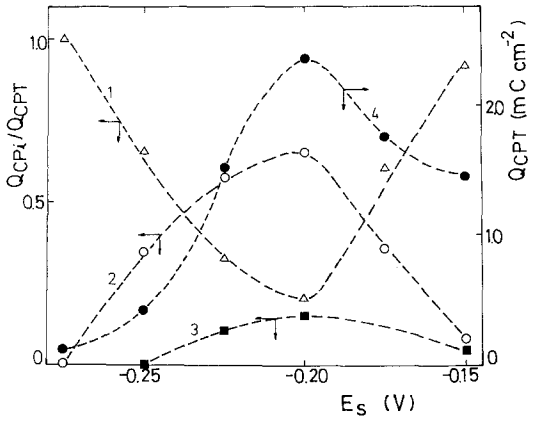

Fig. 8. Charge ratio vs E_s plots (data obtained from Fig. 2). 1. Q_{CPI}/Q_{CPT} vs E_s; 2. Q_{CPII}/Q_{CPT} vs E_s; 3. Q_{CPIII}/Q_{CPT} vs E_s; 4. Q_{CPT} vs E_s.

linearly with log C_{NaOH} ($\partial E_s^{max}/\partial \log C_{NaOH} = -0.059$ V). The same NaOH concentration dependence is obtained for E_p^{API}, E_p^{CPI}, E_p^{CPII} and E_p^{CPIII}. However, the contribution of CPIII with respect to CPII decreases as the C_{NaOH} decreases, CPIII is almost absent when $C_{NaOH} <$ 0.01 mol dm^{-3}.

When E_s is increased at constant τ and v_s, the total cathodic charge (Q_c) reaches a maximum at -0.2 V. At this potential the charge ratio (Q_{CPi} (i = I, II, III)/Q_c) vs E_s plots (Fig. 8) exhibit a minimum for CPI and maxima for CPII and CPIII.

For preset E_s and v_s values, Q_c increases linearly with ln τ for 0.1 and 0.01 mol dm^{-3} NaOH (Fig. 9). This relationship, however, is not fulfilled

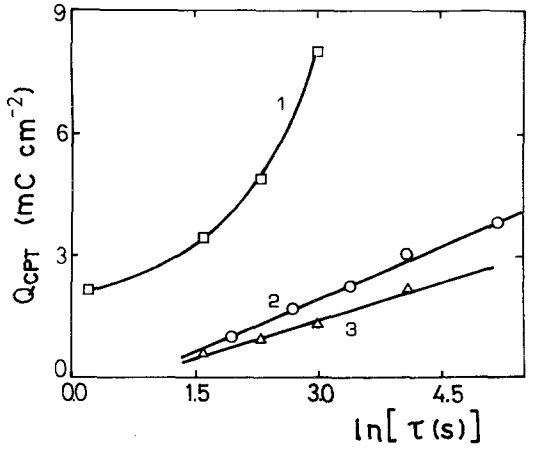

Fig. 9. Q_{CPT} vs τ plots. 1. 1 mol dm^{-3} NaOH; 2. 0.1 mol dm^{-3} NaOH; 3. 0.01 mol dm^{-3} NaOH.

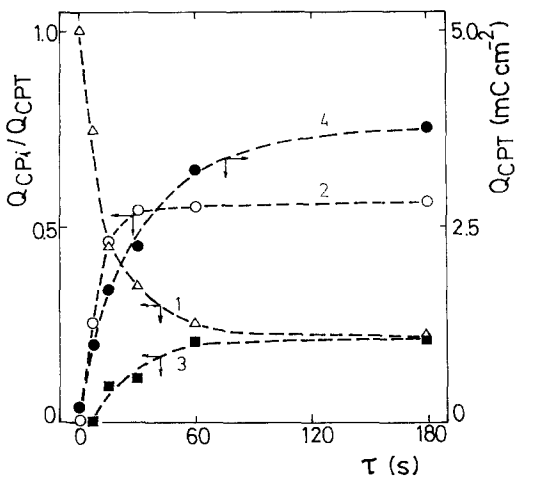

Fig. 10. Charge ratio vs τ plots (data obtained from Fig. 4). 1. Q_{CPI}/Q_{CPT} vs τ; 2. Q_{CPII}/Q_{CPT} vs τ; 3. Q_{CPIII}/Q_{CPT} vs τ; 4. Q_{CPT} vs τ.

for 1 mol dm^{-3} NaOH. This suggests that at large NaOH concentrations, there is a chemical contribution to the film formation. On the other hand, Q_{CPi}/Q_c vs τ plots (for i = I, II, III) exhibit plateaux after about 60 s (Fig. 10). In agreement with the data depicted in Fig. 8, the increase in Q_{CPII} and Q_{CPIII} apparently occurs at the expense of Q_{CPI}.

For constant E_s and τ values the Q_c vs v_s and Q_{CPi}/Q_c vs v_s plots (Fig. 11) show that Q_c increases slightly with v_s but in a complex way, while Q_{CPi}/Q_c (i = I, II, III) reach a constant value for $v_s > 0.2$ V s^{-1} and the Q_{CPIII}/Q_c ratio becomes zero when $v_s < 0.01$ V s^{-1}. This means that the

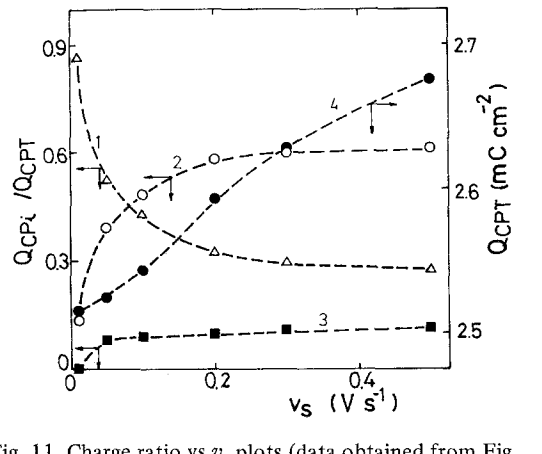

Fig. 11. Charge ratio vs v_s plots (data obtained from Fig. 5). 1. Q_{CPI}/Q_{CPT} vs v_s; 2. Q_{CPII}/Q_{CPT} vs v_s; 3. Q_{CPIII}/Q_{CPT} vs v_s; 4. Q_{CPT} vs v_s.

species related to CPIII is not available at the electrode surface at slow potential sweeps.

Data for 0.01 and 0.1 mol dm^{-3} NaOH indicate that the relative contribution of the processes in the electro-reduction profile depends on the film forming process, as the overall cathodic charge increases linearly with ln τ (Fig. 9), in addition to other processes yielding soluble species. The latter should be associated with CPII and CPIII as these peaks cannot be seen at slow potential sweeps and they exhibit limiting values, when τ exceeds a certain time, because these species attain steady concentration during the applied constant potential.

3.2. *Data obtained with the ring-disc rotating electrode*

When the anodic potential sweep applied to the copper disc exceeds -0.3 V, a net current is detected at the Au-ring electrode either anodic or cathodic with respect to the baseline, depending on the potential applied to the Au-ring (E_r) (Fig. 12). An anodic current is recorded at the Au-ring when $E_r > -0.1$ V and a cathodic one when $E_r < -0.1$ V.

Apparently, the maximum cathodic current at the ring appears when the potential applied to the ring equals that of API. On the other hand, during the negative going potential sweep at the disc the current at the Au-ring is anodic with respect to the baseline for $E_r > -0.4$ V and cathodic for $E_r < -0.5$ V.

The result obtained from the ring-disc rotating electrode demonstrates that soluble species are produced when the potential applied at the electrode is in the ascending branch of API.

There are probably two soluble species, as seen from the ring currents read at different E_r. One of these species is the soluble Cu(I) species which, depending on E_r is either electro-oxidized or electro-reduced at the ring electrode. The potential corresponding to the transition from anodic to cathodic current at the ring is probably related to the Cu/Cu(I) electrode equilibrium potential.

The potential at which the second current contribution turns cathodic lies in the potential range of CPI. The existence of the second Cu(I) soluble species can probaly be related to a pH decrease at the interface.

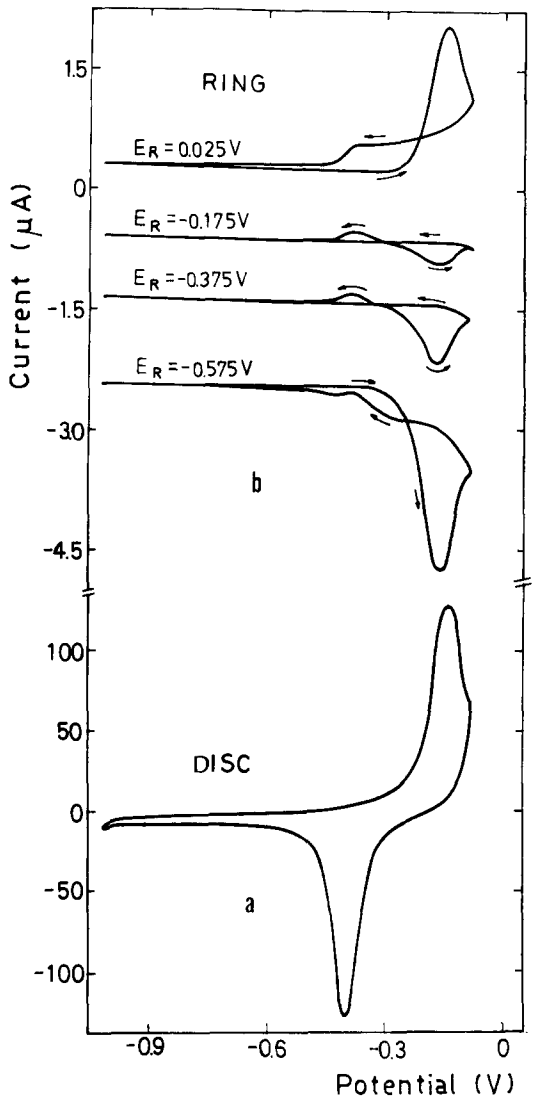

Fig. 12. Rotating Au Ring–Cu disc electrode response. (a) Potentiodynamic E/I profile at the Cu disc; (b) Potentiostatic current response at the Au ring at different applied potentials, 0.1 mol dm^{-3} NaOH; $v_i = 0.1$ V s^{-1}; $\omega =$ 3000 rpm.

The charge recovered at the ring-compensates the $(Q_a - Q_c)$ charge difference measured from the corresponding voltammograms.

3.3. *Electrochemical response of the Cu/Cu_2O redox system prepared from colloidal $Cu(OH)_2$*

When the Cu_2O layer is formed on a vitreous carbon electrode formerly covered with a $Cu(OH)_2$ layer, a very thin Cu/Cu_2O layer of react-

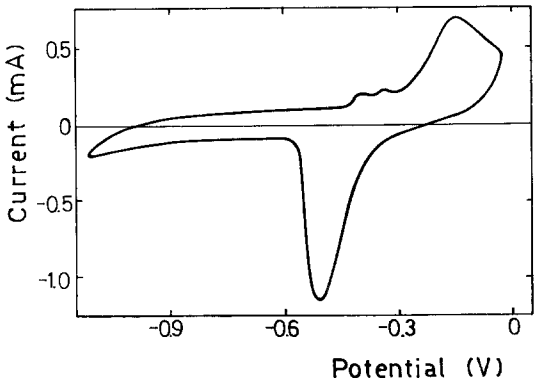

Fig. 13. Potentiodynamic E/I profile obtained at the C(vitreous)/Cu $(OH)_2$ electrode, 0.1 mol dm^{-3} NaOH, $v_s = 0.1$ V s^{-1}.

ing material is provided. In this case, the characteristics of the thin layer of Cu formed from $Cu(OH)_2$ in the initial electro-reduction potential sweep may differ appreciably from those of the bulk Cu electrode.

The voltammogram of the C(vitreous)/Cu/0.1 mol dm^{-3} NaOH in the potential range of the Cu_2O/Cu redox couple (Fig. 13) after 10 min potential cycling exhibits API and CPI as the two main current peaks. These mostly coincide with those already described for bulk Cu electrodes. Nevertheless, the voltammograms run with C(vitreous)/Cu/0.1 mol dm^{-3} NaOH electrodes systematically show an anodic current associated with a redox couple preceeding API (couple I). The cathodic contribution of this couple can be related to the distortion in the ascending portion of CPI. The overall anodic charge involved in these reactions is in the order of or even smaller than a monolayer. Other characteristics of the C(vitreous)/thin Cu layer electrodes which are beyond the scope of the present work will be described in a future publication [13].

4. Discussion

4.1. *General electrochemical characteristics*

The present results together with those reported in previous publications [7, 10, 12] reveal that the potentiodynamic reduction of copper electrodes, previously anodized in the potential range where a Cu_2O layer is formed, depends considerably on the potential perturbation programme. For instance, typical electro-reduction profiles have been presented

i. for a simple RTPS

ii. when the positive going potential sweep is preceded by a potential step

iii. when a potential step is included during the positive going sweep to complete the formation of Cu_2O layer under constant potential conditions and

iv. when the electrode is subjected to a potentiodynamic ageing programme [12].

In case i. only API and CPI are seen but in cases ii.–iv. there is a multiplicity of cathodic peaks which depend on the characteristics of the applied perturbation programme.

In any case, the different electro-reduction E/I profiles reveal that at least three different Cu species are formed during the electro-oxidation of Cu to Cu(I).

In low NaOH concentrations and at constant potential, once the first monolayer has been completed, the electro-reduction film charge increases proportionally to ln τ. However, for 1 mol dm^{-3} NaOH the deviation of the Q_c vs ln τ plot from the straight line relationship (Fig. 9) suggests that, in this case, a combined mechanism involving soluble Cu ionic species contributes to the oxide layer formation. In principle, as a linear Q_c/Q_a relationship can be approached, the anodic layer charge increases also proportionally to ln τ, as is expected for most mechanisms of anodic layer formation [14]. On the other hand, in the course of the anodic reaction soluble Cu(I) and Cu(II) species are formed. Moreover, the formation of Cu(I) soluble species is confirmed by the ring-disc rotating electrode data.

The behaviour of the oxidation process shows two features, one related to the reactions involved in the anodic process and another associated with a possible dependence of the nucleation and growth process of the anodic layer on the perturbation conditions. It is likely that the more reliable information concerning the former comes out from the early stages of the anodic process, while a structural change of the anodic oxide layer associated with the type of perturbation applied to the electrode would at least imply a difference in the kinetics of the dissolution of the different anodic layers yielding Cu(I) species or in the cor-

responding disproportionation reaction at the interface. These processes should change, for instance with the average size of crystallites constituting the anodic film, as the reactivity of the anodic layers should depend also on the ratio of the number of molecules and atoms in contact with the electrolyte solution to molecules and atoms within the crystallites.

4.2. *The initial stage in Cu_2O formation*

Results obtained from the C(vitreous)/Cu electrode indicate that the Cu_2O formation is preceded by an electrochemical reaction associated with a redox couple (couple I), which leads to less than one monolayer of, for example, $Cu(OH)_{ad}$. Couple I has already been observed by other authors but such results were not always reproducible. The reaction was assigned recently to the Cu/CuOH redox couple [11, 15]. The fact that couple I appears on freshly formed thin Cu layers means that the reactivity of the metal surface depends considerably on the structure of the metal layer probably through the work function. These results confirm that the initial stages of the anodic reaction yielding Cu_2O corresponds to OH^- ion discharge on the Cu surface. This type of reaction is considered to be the first step in the electro-oxidation of many metals in aqueous electrolytes and generally it is a fast electrochemical reaction [16].

Otherwise, the results obtained with Cu electrodes support the idea that at least two electrochemically distinguishable reaction sites on the electrode surface participate in the initial electro-oxidation stage. One of these sites denoted as Cu may correspond to those crystallographic sites at the polycrystalline metal surface, whose average reactivity is to a great extent determined by the properties of the bulk metal. Another type of site, represented as Cu^*, may be associated with those produced in freshly electro-reduced thin Cu layers. These sites, quite likely under non-epitaxial conditions, are more reactive than Cu sites towards the OH^- discharge. Furthermore, the occurrence of two energetically different absorption sites suggests that a surface rearrangement of Cu^* into Cu must be possible. Then, the initial stage related to the electroformation of Cu_2O can be formally presented as follows:

$$\begin{array}{lll} Cu^* + OH^- \rightleftarrows Cu^*(OH)_{ad} + e^- & & (1) \\ \downarrow \qquad\qquad\quad \downarrow & & \\ Cu \; + OH^- \rightleftarrows Cu(OH)_{ad} \; + e^- & & (2) \end{array}$$

This reaction scheme explains results previously reported whereby E_a gradually increased within the potential range of the peak API [7], and the electro-reduction profile exhibited for Q_c smaller than a monolayer shows a highly reversible behaviour but for Q_c slightly greater than a monolayer the E/I profile becomes irreversible. The former behaviour can be assigned to the contribution of Reaction 1 while the latter should correspond to Reaction 2.

Reaction 1 is related to couple I, as the reactivity of Cu^* is greater than that of Cu, the formation of $Cu^*(OH)_{ad}$ occurs at a potential more negative than that of $Cu(OH)_{ad}$. The current contribution of Reaction 2 should appear superimposed with that of API in polycrystalline bulk Cu electrode and consequently in this case it is not observable under conventional RTPS measurements.

Reactions 1 and 2 imply two possible reorganisation reactions, one involving Cu^* into Cu, and another $Cu^*(OH)_{ad}$ into $Cu(OH)_{ad}$. Therefore, the initial stage of Cu electro-oxidation involving fresh Cu electrode surfaces can be explained in terms of a square reaction scheme. Accordingly, this stage should be considerably dependent both on the history of the metal phase and on the perturbation conditions applied to the electrode. The degree of hydration of the film forming species should depend on the pH, as already discussed for other O and OH^- containing anodic films [16].

4.3. *The stages related to bulk Cu_2O formation*

The next step is the formation of Cu_2O, from $Cu(OH)_{ad}$. In principle, both $Cu^*(OH)_{ad}$ and $Cu(OH)_{ad}$ can react similarly to yield Cu_2O. This suggests that on the time scale of the present experiments, either the $Cu^*(OH)_{ad}$ to $Cu(OH)_{ad}$ conversion is too fast, or the energy involved in the Cu_2O formation is sufficiently large that the Cu_2O formation and rearrangement process occur simultaneously. Then, the reaction scheme can be written as:

$$\begin{array}{lll} Cu^*(OH)_{ad} & & \\ \downarrow \qquad\qquad \searrow & & \\ \qquad\quad Cu_2^*O + H_2O & & (3a) \\ \qquad\qquad\quad \searrow & & \\ Cu(OH)_{ad} \longrightarrow & Cu_2O & (3b) \end{array}$$

The $Cu^*(OH)$ species in the thin copper film is apparently sufficiently stable that Reaction 1 can be detected. The $Cu^* \rightarrow Cu$ conversion reaction in bulk copper electrodes should, in principle, also be rapid unless the conversion reaction is impeded either by impurities coming from the solution or in the metal, or because of a residual surface energy due to the slow rate of reaching thermal equilibrium of copper [17]. The reaction product involves two Cu_2O species, where Cu_2^*O species participates in an ageing process yielding Cu_2O. This can explain the irreproducibility of the *E/I* profile associated to Reaction 1 when bulk copper electrodes are used.

4.4. *The formation of soluble species during the anodic reaction*

There is evidence through the rotating ring-disc experiments that Cu soluble ionic species are formed during the early stages of Cu_2O formation. These results suggest a chemical dissolution of the $Cu(OH)_{ad}$ species. The formation of Cu(I) species in solution is accounted for by allowing reactions such as

$$2Cu(OH)_{ad} + OH^- \rightleftarrows [Cu_2O_2H^-] + H_2O \quad (4a)$$

$$2Cu(OH)_{ad} + 2OH^- \rightleftarrows [Cu_2O_2^{2-}] + 2H_2O \quad (4b)$$

In the alkaline solution the following partial dissolution of Cu_2O apparently also occurs:

$$Cu_2O + OH^- \rightleftarrows [Cu_2O_2H^-] \quad (5)$$

and

$$Cu_2O_2H^- + OH^- \rightleftarrows [Cu_2O_2^{2-}] + H_2O \quad (6)$$

where the species within brackets denote possible Cu(I) ionic species. The concrete evidence for Cu(I) soluble species in Cu_2O formation comes both from the rotating ring-disc electrode data and the anodic–cathodic charge difference in the voltammogram run at different E_a.

The formation of $[Cu_2O_2^{2-}]$ species should initially prevail but as the Cu_2O formation proceeds, a change in the local pH should promote the contribution of the species $[Cu_2O_2H^-]$. As in the case of $Cu/[CuO_2]^{2-}$ and $Cu/[CuO_2H]^-$ redox couples, the equilibrium potential of the hypothetical $[Cu_2O_2H]^-/Cu$ couple should be more negative than that of the $Cu_2O_2^{2-}/Cu$ redox couple.

The appearance of Cu(I) species either from Cu(OH) or Cu_2O implies the participation of disproportionation reactions in the diffusion layer yielding soluble Cu(II) and Cu^0. As soluble Cu(I) species are rather unstable, one possible reaction in the alkaline electrolyte is:

$$[Cu_2O_2H^-] \rightarrow Cu + CuO_2H^- \quad (7)$$

$$[Cu_2O_2^{2-}] \rightarrow Cu + CuO_2^{2-} \quad (8)$$

where Cu atoms can, in principle, be further electro-oxidized and contribute in part to the Cu_2O film growth.

Soluble Cu(II) species can also be formed from either $Cu(OH)_{ad}$ by

$$Cu(OH)_{ad} + OH^- \rightarrow Cu(OH)_2 + e^- \xrightarrow{OH^-} CuO_2H^- + H_2O \quad (9)$$

or Cu_2O by

$$Cu_2O + 4OH^- \rightarrow 2CuO_2H^- + H_2O + 2e^- \quad (10)$$

Soluble Cu(II) species are clearly present as the electrode reduction voltammograms as described further on.

The yield of soluble Cu ionic species is considerably dependent upon the type of potential perturbation applied to the electrode, namely, a potential step or a linear potential sweep. In the former case, the maximum yield in Cu(I) soluble species appears when the potential E_s is about the middle of the ascending branch of API, while in the latter, it coincides closely with the potential of API. This difference may be related to the fact that the thickness of the Cu_2O layer depends on whether it grows at constant potential or during a linear potential sweep and that accordingly there is an apparent change of the nucleation and growth mechanism. The results suggest that the layer formed at a constant potential is thicker and rougher than that formed during a linear potential sweep. Therefore, the difference in yield of Cu ionic species can be explained in terms of a dissolution process depending either on the growth characteristics of the layer or on the solubility of the species prevailing under different potential perturbation conditions.

The difference between the density of crystalline Cu_2O and that anodically formed can be interpreted either by assuming that the growth of the Cu_2O layer occurs in patches that gradually spread

to form a base structure or by concluding that Cu_2O and CuOH species are simultaneous components of the anodic layer. The former model was used for calculating the optical characteristics of the Cu_2O layer which should not be linear with film thickness, while the latter which better explained the optical data, implies that the Cu_2O to Cu(OH) ratio species in the layer is time dependent.

Therefore, the properties derived from anodic layers produced potentiostatically cannot be extended completely to those which are formed under transient conditions.

4.5. *The multiplicity of the reduction E/I profile*

The multiplicity of current peaks in the reduction *E/I* profile can be easily explained in terms of the various products formed either electrochemically or chemically during the oxidation process. Therefore, the anodic layer produced under transient conditions should be a mixture of various species, namely $Cu(OH)_{ad}$, $Cu^*(OH)_{ad}$ and Cu_2O. These species together with soluble Cu(II) and Cu(I) species should, in principle, be detected through the reduction *E/I* profile. The situation, however, becomes more involved because the relative ratio of each component in the anodic layer depends on the amount of product formed, that is on the time spent in forming the layer, which includes E_a and v_s in the potentiodynamic runs and E_s and τ in the anodic layer formed at constant potential. Thus, when $Q_a \to 0$ and $t \to 0$, the prevailing species are associated with the $Cu(OH)_{ad}$ species, while when $Q_a \to$ multilayer and $t \to \infty$, the main product is Cu_2O. The different straightline portions of the Q_a vs E_a and Q_c vs E_a linear plots, at a constant v_s, derived from potentiodynamic runs (Fig. 14) suggest the prevalence of different structures of the anodic layer according to Q_a.

Consequently, CPI and CPII constitute complex peaks where the reduction charges of $Cu(OH)_{ad}$, Cu_2^*O and Cu_2O partially overlap. Therefore, the reduction profile should involve, in addition to the contribution specifically related to the $Cu^*(OH)_{ad}$ species (couple I), two cathodic ones associated with the reduction of Cu_2O and Cu_2^*O and the electrodeposition of Cu from soluble Cu(II) species. The overall reaction of Cu_2O and Cu_2^*O is represented by the reaction:

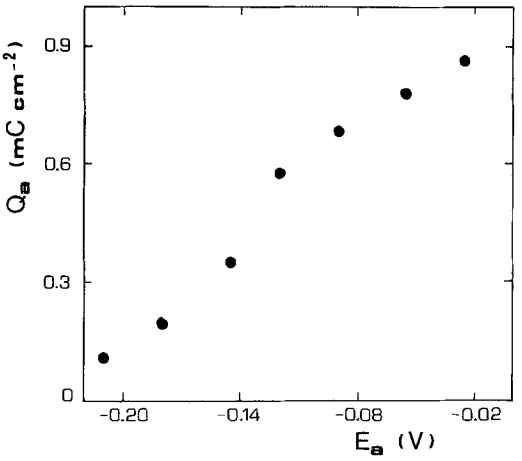

Fig. 14. Q_a vs E_a plot resulting from *E/I* profiles run with different E_a. 0.1 mol dm^{-3} NaOH, $v_s = 0.1$ V s^{-1}.

$$\begin{array}{l} Cu_2^*O + H_2O + 2\,e^- \\ \downarrow \qquad\qquad\qquad \searrow \\ Cu_2O + H_2O + 2\,e^- \end{array} \quad 2Cu + 2OH^- \qquad (11)$$

CPI can be assigned to the reduction of $Cu(OH)_{ad}$ and Cu_2^*O and CPII to the reduction of aged Cu_2O. Reaction 11 is probably related to a transition which requires a nucleation and growth mechanism. As an epitaxial growth of the copper lattice is, in principle, impossible due to the crystallographic differences between Cu and Cu_2O, Reaction 11 presumably occurs by a scheme analogous to Steps 1 and 2

$$\begin{array}{l} Cu_2O + H_2O + 2\,e^- \to 2Cu^* + 2OH^- \\ \uparrow \qquad\qquad\qquad\quad \downarrow \\ Cu_2^*O + H_2O + 2\,e^- \to 2Cu \end{array} \qquad (12)$$

On the other hand, the electrodeposition of Cu from soluble Cu(II) species occurs in the potential range of CPIII. The corresponding charge depends on the anodization time and on the alkali concentration, which determines the CuO_2^{2-}/CuO_2H^- concentration ratio in solution. As in the case of Cu_2O electroreduction, the overall reaction can be represented by

$$HCuO_2^- \underset{-OH}{\overset{OH^-}{\rightleftharpoons}} CuO_2^{2-} \xrightarrow[+\,2H_2O]{+\,2e^-} \begin{array}{l} Cu^* + 4OH^- \\ \downarrow \\ Cu \end{array} \qquad (13)$$

The contribution of the Cu^* to Cu surface reaction in both cases is considerably enhanced when a thin copper layer is employed.

In conclusion, the potentiodynamic behaviour of copper in alkaline electrolyte reveals that the process involves a series of complex reactions including electrochemical and chemical stages occurring both consecutively and competitively. This reaction formalism leaves open the participation of processes controlled by phase growth associated with conductivity changes in the oxide layer. During the oxide layer growth at constant potential differential dehydration processes yield an OH/O ratio changing through the oxide layer thickness should also occur once the latter exceeds the length in which the electron tunnelling probability is sufficiently large.

Acknowledgements

INIFTA is sponsored by the Consejo Nacional de Investigaciones Científicas y Técnicas, the Universidad Nacional de La Plata and the Comisión de Investigaciones Científicas (Provincia de Buenos Aires).

References

[1] B. Miller, *J. Electrochem. Soc.* **116** (1969) 1675.
[2] M. J. Dignam and D. B. Gibbs, *Can. J. Chem.* **48** (1970) 1242.
[3] N. A. Hampson, J. B. Lee and K. I. MacDonald, *J. Electroanal. Chem.* **32** (1971) 165.
[4] J. Ambrose, R. G. Barradas and D. W. Shoesmith, *ibid.* **47** (1973) 47.
[5] D. W. Shoesmith, T. E. Rummery, D. Owen and W. Lee, *J. Electrochem. Soc.* **123** (1976) 790.
[6] V. Ashworth and D. Fairhurst, *ibid.* **124** (1977) 506.
[7] A. M. Castro Luna de Medina, S. L. Marchiano and A. J. Arvía, *J. Appl. Electrochem.* **8** (1978) 121.
[8] S. Fletcher, R. G. Barradas and J. D. Porter, *J. Electrochem. Soc.* **125** (1978) 1960.
[9] M. Yamashita, K. Omura and D. Hirayama, *Surf. Sci.* **96** (1980) 443.
[10] S. L. Marchiano, C. I. Elsner and A. J. Arvía, *J. Appl. Electrochem.* **10** (1980) 365.
[11] J. M. M. Droog, C. A. Alderliesten, P. T. Alderleisten and G. A. Bootsma, *J. Electrochem. Soc.* **111** (1980) 65.
[12] M. E. Martins and A. J. Arvia, *J. Electroanal. Chem.* in press.
[13] M. R. Gennero de Chialvo, S. L. Marchiano and A. J. Arvia, in preparation.
[14] K. Hauffe, 'Oxidation of Metals', Plenum Press, New York (1965).
[15] J. M. M. Droog and B. Schleuter, *J. Electroanal. Chem.* **112** (1980) 387.
[16] A. J. Arvía, Proceedings 8th International Congress of Metallic Corrosion, Vol. III, Mainz, Germany, September 1981, p. 2065.
[17] J. O'M. Bockris and E. Buck, 'Structure and Properties of Metal Surfaces', Maruzen Co., Tokyo (1973).